Electrochemistry Communications 160 (2024) 107665

Contents lists available at ScienceDirect

Electrochemistry Communications

journal homepage: www.elsevier.com/locate/elecom

Full Communication

Fluoropyridine-medicated zeolite templating method for N/F co-doped carbon with high electrocatalytic performance on oxygen reduction reaction

Yurika Taniguchi [a], Shinya Kokuryo [a], Ryuji Takada [a], Xinran Yang [a], Koji Miyake [a,b,*], Yoshiaki Uchida [a], Norikazu Nishiyama [a,b]

[a] Division of Chemical Engineering, Graduate School of Engineering Science, Osaka University, 1-3 Machikaneyama, Toyonaka, Osaka 560-8531, Japan
[b] Innovative Catalysis Science Division, Institute for Open and Transdisciplinary Research Initiatives (ICS-OTRI), Osaka University, Suita 565-0871, Japan

ARTICLE INFO

Keywords:
Heteroatom doped carbon
Electrocatalyst
Zeolite templating method
Oxygen reduction reaction

ABSTRACT

Heteroatom-doped carbons have attracted increasing attention in recent years as inexpensive high-performance electrocatalytic materials owing to their electrical properties. A precisely controlled synthesis method for heteroatom-doped carbons is important to improve their performance and expand their applications. In this study, we developed a fluoropyridine-medicated zeolite templating method for Nitrogen/Fluorine (N/F) co-doped carbons. The N/F co-doped carbons showed better catalytic performances for oxygen reduction reaction (ORR) than N-doped carbon prepared using pyridine. In particular, the optimized N/F co-doped carbon exhibited a higher half-wave potential (0.87 V vs. RHE) than commercial Pt-loaded carbon black and N/F co-doped carbons reported in the literature. The comparative studies using various N/F co-doped carbons revealed that semi-ionic bonded C-F might improve ORR activity. In contrast, the contribution from covalent or ionic C-F to improving ORR activity would be negligible.

1. Introduction

Recently, heteroatom-doped carbon has received increasing attention [1,2]. Doping graphene networks with heteroatoms results in properties not observed for pure carbon. When a heteroatom with a different size or electronegativity from carbon replaces some of the carbon atoms in the graphene lattice, structural distortion or bias in the charge density distribution occurs in the graphene network, leading to the formation of active sites on the heteroatom-doped carbons [3,4]. The charge density distribution can be controlled by selecting the type and number of heteroatoms as dopants, making it possible to synthesize carbon materials for various applications [3]. The electrochemical field is one of the fields where heteroatom-doped carbon is expected to be put to practical use because of its high electrical conductivity and chemical stability [5,6]. In particular, it is known that heteroatom-doped carbon has been used in the oxygen reduction reaction (ORR), a cathodic reaction in fuel cells and air batteries. Although platinum catalysts, commonly used today as electrocatalysts for these reactions, have high performance, there are some problems regarding low chemical durability and very high cost. These challenges have hindered the commercialization of next-generation power generation devices [7]. Therefore, there is a need to develop inexpensive and highly durable alternative catalysts to replace Pt catalysts [8]. Studies on alternative catalysts, such as non-precious metals [9–11] and alloy catalysts [12–14], have been reported. Unlike these catalysts, heteroatom-doped carbon catalysts have the advantages of low cost and chemical stability because they do not contain metals.

Most reports on heteroatom-doped carbon materials have focused on nitrogen [15–17], boron [17–19], and phosphorus [17,20,21] as the heteroatoms. Recently, halogen elements have emerged as promising dopants. In particular, F atoms with high electronegativity are inserted at the edges of graphene lattices to form semi-ionic C-F bonds [22], creating active sites [23]. In particular, semi-ionic C-F bonds increase the conductivity of N/F co-doped carbon by increasing the degree of C-C polarization, causing changes in the electrical and spin densities, and lowering the overvoltage and resistance [24]. Furthermore, it has been reported that F-doping weakens the O-O bond in the ORR process, thus preferentially promoting four-electron reactions [25–28].

* Corresponding author at: Division of Chemical Engineering, Graduate School of Engineering Science, Osaka University, 1-3 Machikaneyama, Toyonaka, Osaka 560-8531, Japan.
E-mail address: kojimiyake@cheng.es.osaka-u.ac.jp (K. Miyake).

https://doi.org/10.1016/j.elecom.2024.107665
Received 5 December 2023; Received in revised form 28 December 2023; Accepted 8 January 2024
Available online 10 January 2024

In our previous study [29,30], we successfully developed edge-site-rich and highly active N-doped carbon catalysts [31,32] using the zeolite template method [33]. This method can selectively introduce N species at the edge sites, such as pyridinic N and valley N [1,26,27,34], nitrogen species effective for ORR activity, into the carbon substrate. Inspired by our recent results, we expect that the use of raw materials, including both N and F for the zeolite templating method, may lead to the controlled synthesis of N/F co-doped carbon with suitable chemical states of N and F species for high electrocatalyst performance. In this study, we synthesized N/F co-doped carbon as an electrocatalyst with high activity using a zeolite templating method with fluoropyridine as a raw material.

2. Experimental

2.1. Materials

Pyridine, 2-propanol, 4 M NaOH, 5 M HCl, 5 % Nafion™ dispersion solution and 0.1 M KOH were purchased from Wako Pure Chemical Industries, while 2-fluoropyridine and 3-fluoropyridine were purchased from Tokyo Chemical Industry. H^+ type Y zeolite (FAU) with a SiO_2/Al_2O_3 ratio of 7.2 was purchased from Tosoh Corporation.

2.2. Synthesis of carbon materials

The deposition and removal of zeolite procedures were performed referring to our previous work [30]. Typically, the Y zeolite (0.3 g) was heated under N_2 atmosphere to a certain temperature T (=600, 700, 800 and 900 ℃) and the temperature was maintained for 1 h. Then, a vapor of 2-fluoropyridine was fed into the furnace at the saturated pressure at 0 ℃, and the vapor deposition treatment was performed for a certain time t (4, 5 and 6 h). The composite of carbon and zeolite was named "CNF/Z-T ℃-t h", where T and t represent the deposition temperature and time, respectively.

The composite was immersed in 4 M NaOH solution at 180 ℃ overnight. The resultant powder was recovered by filtration, and washed with deionized water. Subsequently, 5 M HCl solution was added to the resultant powder. Finally, the resultant powder was washed again with deionized water until the solution was neutral. The wet powder was then dried overnight at 90 °C. The dry powder was named "CNF-T ℃-t h". In addition, recarbonization was performed under N_2 atmosphere at 1100 ℃ for 3 h. The recarbonized sample is denoted as "CNF-T ℃-t h-recarb".

As comparisons, we synthesized carbons by similar procedures using pyridine or 3-fluoropyridine instead of 2-fluoropyridine, and the obtained samples were donated as "3-CNF-recarb" and "CN-recarb". respectively. The deposition temperature and time were 800 ℃ and 5 h, respectively.

2.3. Material characterization

Energy-dispersive X-ray spectroscopy (EDX) was performed using a JEOL JCM-7000 to confirm the existence of the zeolite components Si and Al. The grain size and shape of the samples were observed using a Hitachi H-800 transmission electron microscope (TEM). X-ray diffraction (XRD) was performed on a PANalytical X'Pert-MDR diffractometer using Cu Kα radiation to record the crystal structure. Nitrogen adsorption measurements were performed at 77 K using a Microtrac-BEL BELSORP min X. The structures of the carbon catalyst were analyzed using Raman spectroscopy (LabRAM HR-800, Horiba, Ltd., Kyoto, Japan). Raman spectra of the samples were recorded using a confocal Raman microscope (LabRAM HR-800, Horiba, Ltd., Kyoto, Japan). X-ray photoelectron spectroscopy (XPS) was performed using a JEOL JPS-9000MX spectrometer with Mg Kα radiation (10 kV, 10 mA) as the energy source to obtain C 1 s, N 1 s and F 1 s spectra.

2.3.1. Electrochemical tests

Electrochemical activity was measured in a three-electrode cell using a Bi-Potentiostat (BAS) referring to our previous work [35]. A rotating ring disk electrode (RRDE) (glassy carbon (GC) ring-disk) (diameter: 4 mm) loaded with each sample was used as the working electrode, a Hg/Hg_2Cl_2 (saturated KCl) electrode as the reference electrode, and a graphite rod as the counter electrode. The catalyst ink was prepared by dispersing each sample (8.8 mg) in a mixture including 0.8 mL deionized water, 0.1 mL of Nafion solution, and 0.1 mL of 2-propanol. The RRDEs were then coated with 8 μL of ink and dried in air. The potential conversion from a saturated calomel electrode (SCE) to a reversible hydrogen electrode (RHE) was calculated using the following Nernst equation:

$$E_{RHE} = E_{SCE} + 1.0083(at 0.1MKOH)$$

The ORR activity was evaluated by linear sweep voltammetry (LSV) in O_2-saturated 0.1 M KOH solution in the 0.2–1.0 V (vs. RHE) range at a scan rate of 10 mV s^{-1}. We performed 20 cycles of LSV measurements for each sample to obtain the stabilized results and used the data from the last cycle.

3. Results and discussion

The results of the EDX analysis (Table S1) indicate that Si and Al, which are the main components of zeolites, were not almost detected in the CNF-800 °C-5 h-recarb, which means that zeolite was removed by base and acid treatment. The CHN elemental analysis (Table S2) revealed that the amount of nitrogen in each sample was approximately 2–4 wt%. No significant differences in the nitrogen content were observed for all the samples. TEM observations confirmed that pores were formed after zeolite removal, as shown in Fig. 1. The shape and particle size (~1 μm) for all the materials even after carbonization, zeolite removal, and recarbonization were similar to those of the template zeolite. Similar trends were observed in both the EDX analysis (Table S1) and TEM observations (Fig. S1-S3) were obtained for other samples prepared at different deposition temperatures, times, and raw materials. The XRD patterns (Fig. S4) showed peaks similar to those of zeolite (H/Y) even after carbonization, indicating that carbon materials were formed while the zeolite retained its structure. These results suggest that the zeolite acted as a template. Nitrogen adsorption measurements are shown in Fig. 2. It was confirmed that the amount of nitrogen adsorption on CNF-800 °C-5 h, from which the zeolite was removed by the base and acid treatments, increased significantly. The porosity of all the samples increased after base and acid treatments, as shown in Fig. S5 (a) and (b), which confirms the generation of pores derived from zeolite templates for all samples. After recarbonization, the amount of adsorption in the micropore region decreased, and the number of mesopores increased compared to those after the base and acid treatments. The decrease in microporosity may be due to the high-temperature recarbonization treatment, which aligned the graphene microscale defects as a graphene lattice and shrieked the micropores. Meanwhile, the increase in mesoporosity may be due to the elimination of the F species. A similar phenomenon occurred when F-containing raw materials were carbonized in some papers [36]. As for N-doped carbon without F species, only a decrease in the porosity was observed after recarbonization, as shown in Fig. S5(b) and (c). This is because only pore shrinkage occurred because of the absence of F species. However, the porosities of all F-containing samples did not improve after recarbonization. This may be because an increase in the elimination of F species and a decrease by shrinkage at high temperatures would be comparative.

Fig. 3 shows the results of the LSV measurements when the RRDE was rotated at 1600 rpm in O_2-saturated 0.1 M KOH. Similar onset potentials were obtained for all the samples, even when the carbonization temperature, carbonization time, and raw material were changed. Meanwhile, a large difference was observed in the current density values

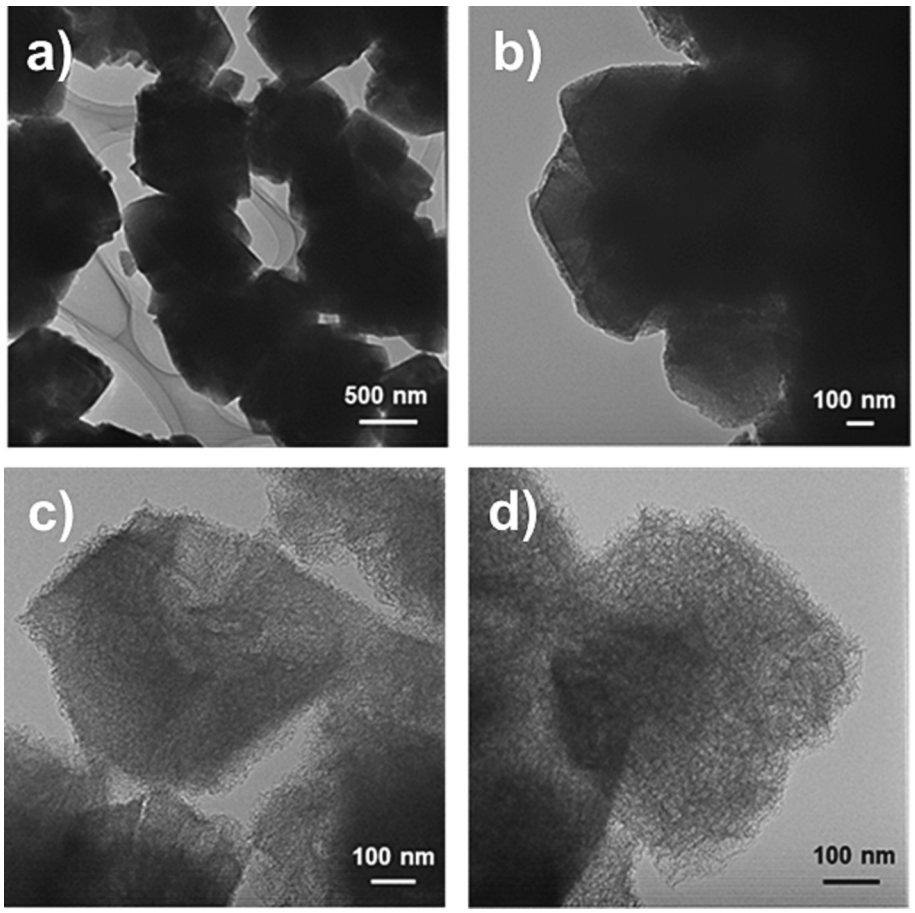

Fig. 1. TEM images of (a) H/Y, (b) CNF/Z-800 °C-5 h, (c) CNF-800 °C-5 h and (d) CNF-800 °C-5 h-recarb.

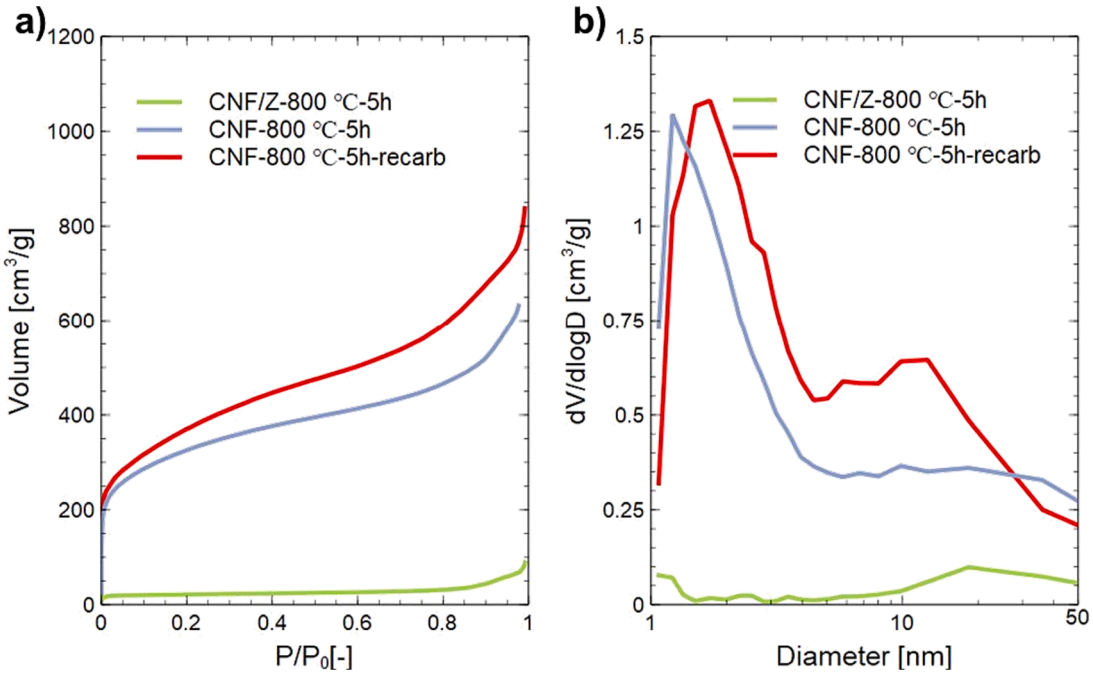

Fig. 2. (a) N_2 adsorption isotherms and (b) pore size distributions of CNF/Z-800 °C-5 h, CNF-800 °C-5 h and CNF-800 °C-5 h-recarb.

(Table S3). CNF-800 °C-5 h-recarb showed the highest onset potential and current density value. These values were higher than those of N/F co-doped carbons for ORR in previous reports as listed in Table S4. In particular, the half-wave potential of CNF-800 °C-5 h-recarb was much better than those of N/F co-doped carbons for ORR in previous reports. Furthermore, the CNF-800 °C-5 h-recarb exhibited high stability and

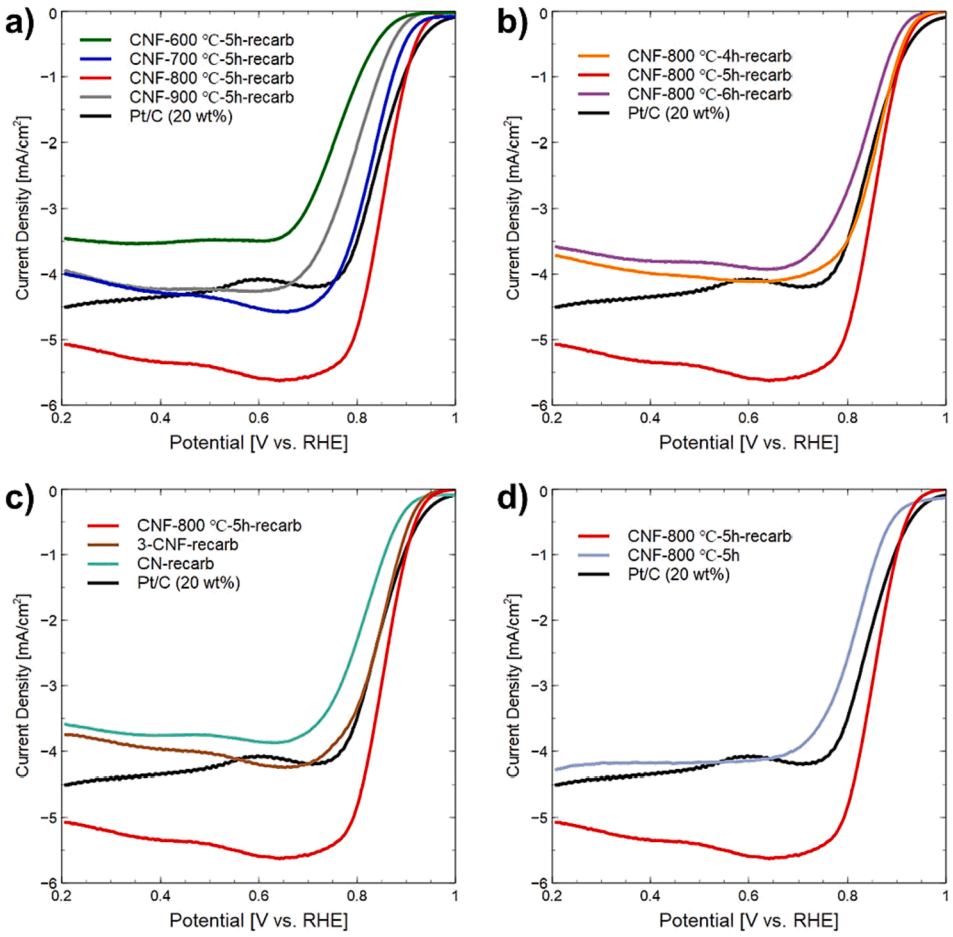

Fig. 3. LSV curves of (a) samples synthesized at various carbonization temperatures, (b) samples synthesized at various carbonization times (c) samples synthesized at various raw materials and (d) before and after recarbonization in the oxygen-saturated 0.1 M KOH solution at a scan rate of 5 mV s^{-1}. As a comparison, results for a carbon catalyst with 20 wt% platinum loading are shown.

methanol tolerance (Fig. S6). Next, to investigate in detail the differences in activity depending on the raw material, we focused on three samples: CNF-800 °C-5 h-recarb, 3-CNF-recarb, and CN-recarb. Using these LSV measurements, we analyzed the number of transferred electrons during the measurement, as shown in Fig. S7: the desired four-electron reaction was preferred for the CNF-800 °C-5 h-recarb and 3-CNF-recarb, whereas the electron transfer number for CN-recarb was lower than that for the N/F co-doped carbons. Thus, it can be inferred that F doping preferentially promoted the four-electron reaction. The large difference in current density between the CNF-800 °C-5 h-recarb and 3-CNF-recarb suggests that the binding state of F is importantly related to the current density of the N/F co-doped carbons. Furthermore, because there was no significant difference in the onset potential among the three samples, it was expected that the presence or absence of F and its bonding state would not significantly affect the onset potential. Fig. 4 (d) shows the changes in activity before and after recarbonization. Both the onset potential and current density were enhanced by recarbonization. In particular, a large increase in the current density was observed. The improvement in the catalytic activity after recarbonizaition may be due to both the increase in the porosity (Fig. 2) and the change of chemical states after recarbonizaition. Finally, the activity of the CNF-800 °C-5 h-recarb was compared with a 20 wt% platinum-supported carbon catalyst (Pt/C 20 wt%). CNF-800 °C-5 h-recarb showed activity comparable to that of the platinum catalyst. The half-wave potential and current density exceeded those of a platinum catalyst.

The structure of the carbon catalyst was investigated by Raman spectroscopy as shown in Fig. S8. Graphene exhibits two characteristic peaks at 1000 ~ 2000 cm^{-1}. One is the D band (1350 cm^{-1}) derived from sp^2 graphitic crystallites and the other is the G band (1580 cm^{-1}) derived from defects. Therefore, I_D/I_G, calculated from the intensity ratio of each peak, represents the degree of defects. There was no significant difference in I_D/I_G among the three samples synthesized from the three different raw materials, but the I_D/I_G of CN was slightly smaller than that of CNF. This may be attributed to the defect formation due to fluorine doping.

The surface binding of each sample was examined by XPS measurements, and the results for N 1 s showed that all samples had Center N, Pyridinic N, and Valley N peaks as shown in Fig. 4 (Center N: 401.0 eV, Pyridinic N: 398.5 eV, Valley N: 401.9 eV) [34,37]. After recarbonation, the ratios of Pyridinic N and Valley N decreased. This may be due to the alignment of the graphene lattice by recarbonization. Comparing the amount of nitrogen species in the samples after recarbonization, the highest ratio of Pyridinic N and Valley N were found in the CNF-800 °C-5 h-recarb; however, there was no significant difference in the ratios among the three samples (Table S5). The fact that there was no significant difference in the ratio of Pyridinic N and Valley N among the three samples synthesized by the zeolite templating method suggests that there was no significant difference in the onset potentials among the three samples. XPS measurements of F 1 s are shown in Fig. 5: the F 1 s spectra are separated into Ionic, Semi-ionic, and Covalent C-F bonds at each binding energy (Ionic C-F bond: 686.0 eV, Semi-ionic C-F bond: 687.3 ~ 688.0 eV, Covalent C-F bond: 689.4 eV) [24,25]. The CNF-800 °C-5 h-recarb was found to have a lower ratio of Semi-ionic C-F bonds than the 3-CNF-recarb (Table S6). This is contrary to the

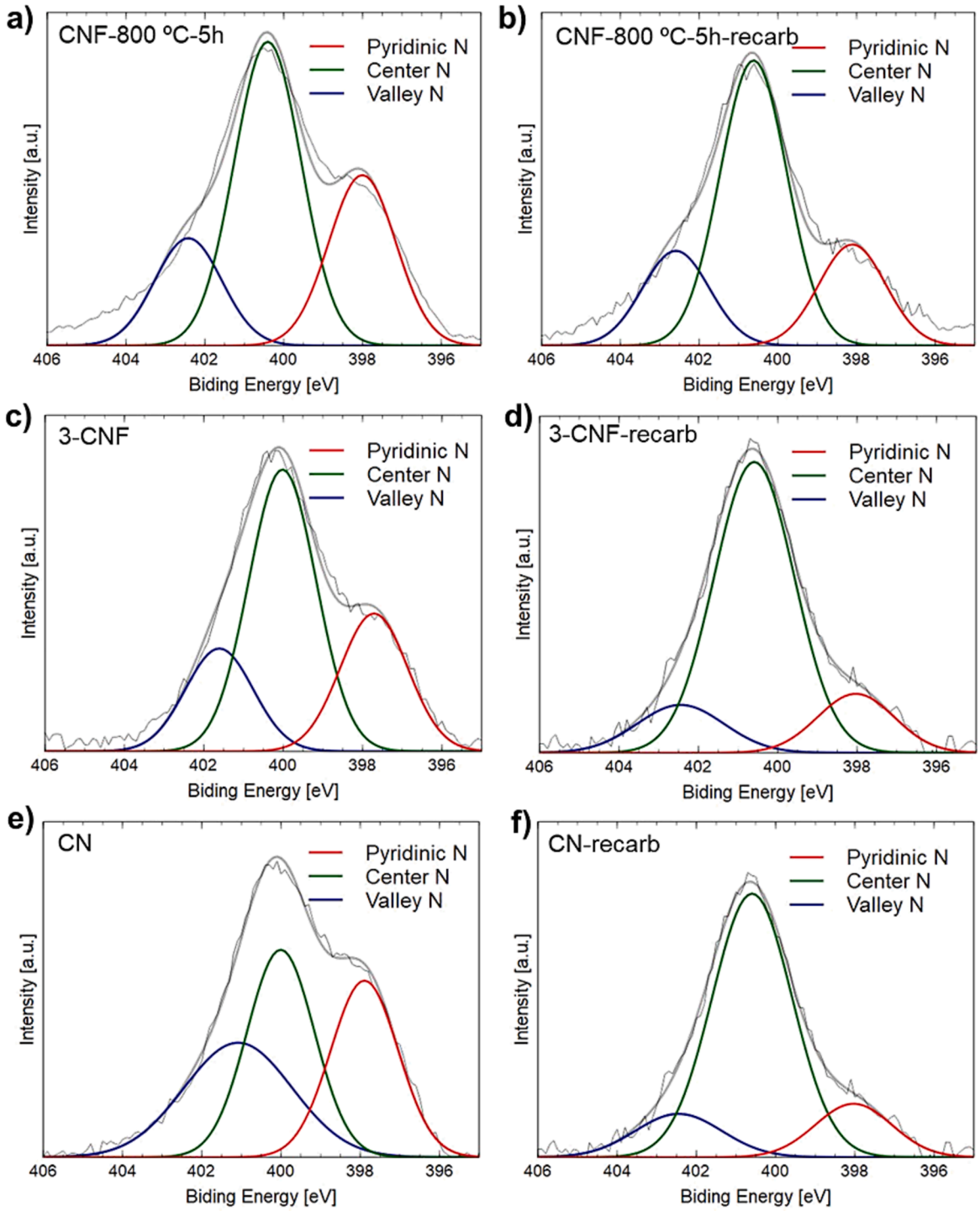

Fig. 4. N 1 s XPS profiles of (a) CNF-800 °C-5 h, (b) CNF-800 °C-5 h-recarb, (c) 3-CNF, (d) 3-CNF-recarb, (e) CN and (f) CN-recarb.

theoretically based result that the CNF-800 °C-5 h-recarb had a higher current density values than the 3-CNF-recarb. However, the majority of both samples were dominated by Semi-ionic C-F bonds, and the Semi-ionic C-F must have contributed to the higher current values. In addition, 3-CNF-recarb must contain a small amount of Covalent-C-F, although no peak of Covalent-C-F was observed in 3-CNF-recarb. In these samples with very low fluorine content, the intensity of the XPS spectrum is low, making it hard to accurately characterize the samples by only XPS. Compared to the samples before recarbonation, CNF-800 °C-5 h and 3-CNF had Covalent C-F bonds whose peak intensity decreased after recarbonation. It is expected that the recarbonization changed the structure of the graphene lattice and the charge density distribution, which converted the Covalent C-F bonds to Ionic bonding properties. This phenomenon may have caused the enhanced current values after recarbonization.

4. Conclusions

We synthesized N/F co-doped carbons by a zeolite templating method using fluoropyridine as a deposition source. The N/F co-doped carbons showed better catalytic performances on ORR than N doped carbon prepared using pyridine. Significant improvements by F-doping

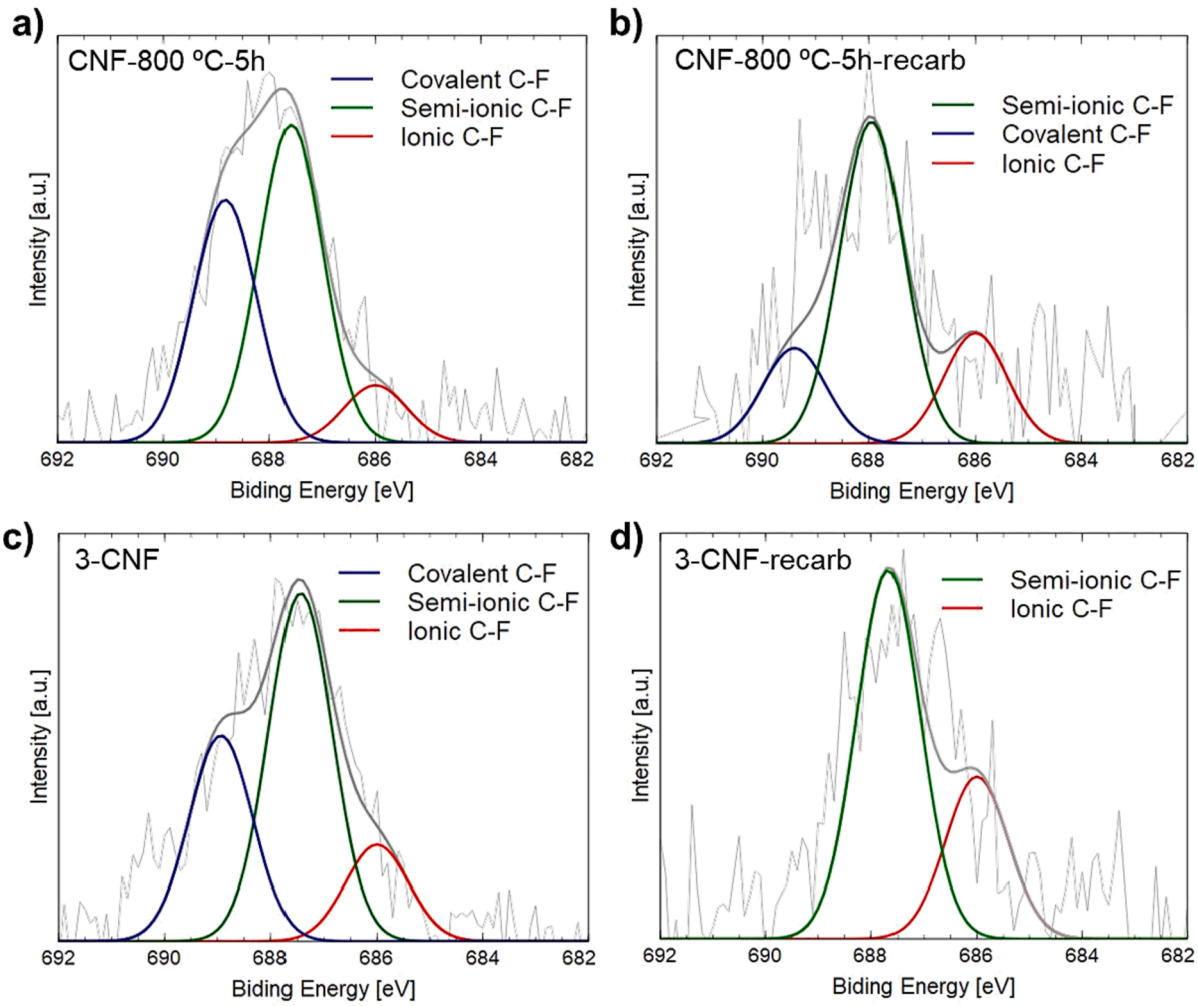

Fig. 5. F 1 s XPS profiles of (a) CNF-800 °C-5 h, (b) CNF-800 °C-5 h-recarb, (c) 3-CNF and (d) 3-CNF-recarb.

were observed in current density and electron transfer numbers. XPS measurements of N 1 s confirmed that the N/F co-doped carbons possessed Center N, Pyridinic N, and Valley N with a similar distribution to the N doped carbon, therefore, F species boosted ORR catalytic performance. The comparisons revealed that Semi-ionic bonded C-F might boost catalytic performance on ORR while Covalent or Ionic C-F would not boost it. This work provides a new direction for the design of metal-free heteroatom co-doped carbon electrocatalysts for ORR.

CRediT authorship contribution statement

Yurika Taniguchi: Writing – original draft, Methodology, Investigation, Formal analysis, Data curation, Conceptualization. **Shinya Kokuryo:** Writing – review & editing, Methodology, Conceptualization. **Ryuji Takada:** Writing – review & editing, Methodology, Investigation. **Xinran Yang:** Writing – review & editing, Methodology. **Koji Miyake:** . **Yoshiaki Uchida:** Writing – review & editing. **Norikazu Nishiyama:** Writing – review & editing, Supervision, Resources, Funding acquisition.

Declaration of competing interest

The authors declare that they have no known competing financial interests or personal relationships that could have appeared to influence the work reported in this paper.

Data availability

Data will be made available on request.

Acknowledgements

A part of the present experiments was carried out by using a facility in the Research Center for Ultra-High Voltage Electron Microscopy, Osaka University. Raman spectra measurements were supported by Prof. Hiroshi Umakoshi, Assistant Prof. Nozomi Watanabe and Mr. Ward Wakileh.

Appendix A. Supplementary data

Supplementary data to this article can be found online at https://doi.org/10.1016/j.elecom.2024.107665.

References

[1] N. Daems, X. Sheng, I.F.J. Vankelecom, P.P. Pescarmona, Metal-free doped carbon materials as electrocatalysts for the oxygen reduction reaction, J. Mater. Chem. A 2 (2014) 4085–4110, https://doi.org/10.1039/C3TA14043A.
[2] H. Itoi, H. Nishihara, T. Kyotani, Effect of heteroatoms in ordered microporous carbons on their electrochemical capacitance, Langmuir 32 (2016) 11997–12004, https://doi.org/10.1021/acs.langmuir.6b02667.
[3] K.R.D. Kasibhatta, I. Madakannu, I. Prasanthi, Hetero atom doped graphene nanoarchitectonics as electrocatalysts towards the oxygen reduction and evolution reactions in acidic medium, J. Inorg. Organomet. Polym. 31 (2021) 1859–1876, https://doi.org/10.1007/s10904-020-01834-w.

[4] S. Miao, K. Liang, J. Zhu, B. Yang, D. Zhao, B. Kong, Hetero-atom-doped carbon dots: Doping strategies, properties and applications, Nano Today 33 (2020) 100879, https://doi.org/10.1016/j.nantod.2020.100879.
[5] H.C. Pandhurnekar, C.P. Pandhurnekar, N. Sharma, Recent advances in the energy harvesting device technology using hetero-atom doped carbon nanotubes, Mater. Today:. Proc. 73 (2023) 41–49, https://doi.org/10.1016/j.matpr.2022.09.081.
[6] R. Karthikeyan, D.J. Nelson, A. Ajith, S.A. John, Hetero atoms doped carbon dots modified electrodes for the sensitive and selective determination of phenolic anti-oxidant in coconut oil, J. Electroanal. Chem. 848 (2019) 113297, https://doi.org/10.1016/j.jelechem.2019.113297.
[7] M.K. Debe, Electrocatalyst approaches and challenges for automotive fuel cells, Nature 486 (2012) 43–51, https://doi.org/10.1038/nature11115.
[8] Z. Zhu, H. Yin, Y. Wang, C. Chuang, L. Xing, M. Dong, Y. Lu, G. Casillas-Garcia, Y. Zheng, S. Chen, Y. Dou, P. Liu, Q. Cheng, H. Zhao, Coexisting Single-Atomic Fe and Ni Sites on Hierarchically Ordered Porous Carbon as a Highly Efficient ORR Electrocatalyst, Adv. Mater. 32 (2020) 2004670, https://doi.org/10.1002/adma.202004670.
[9] L. Gao, H. Zhang, Z. Zhang, Ingeniously introducing of boron to adjust hetero-atoms and their bonding with cobalt for improving the catalysis of oxygen reduction reaction, J. Solid State Chem. 289 (2020) 121523, https://doi.org/10.1016/j.jssc.2020.121523.
[10] M. Zhu, J. Nong, P. Xie, A.S. Zhu, M.Z. Rong, M.Q. Zhang, Well-dispersed CoO embedded in 3D N-S-doped carbon framework through morphology-retaining pyrolysis as efficient oxygen reduction and evolution electrocatalyst, Electrochim. Acta 295 (2019) 624–631, https://doi.org/10.1016/j.electacta.2018.10.200.
[11] Y. Li, Z. Li, Y. Wu, H. Wu, H. Zhang, T. Wu, C. Yuan, Y. Xu, B. Zeng, L. Dai, Carbon particles co-doped with N, B and Fe from metal-organic supramolecular polymers for boosted oxygen reduction performance, J. Power Sources 412 (2019) 623–630, https://doi.org/10.1016/j.jpowsour.2018.11.091.
[12] M.S. Garapati, R. Sundara, Highly efficient and ORR active platinum-scandium alloy-partially exfoliated carbon nanotubes electrocatalyst for Proton Exchange Membrane Fuel Cell, Int. J. Hydrogen Energy 44 (2019) 10951–10963, https://doi.org/10.1016/j.ijhydene.2019.02.161.
[13] F. Fouda-Onana, S. Bah, O. Savadogo, Palladium–copper alloys as catalysts for the oxygen reduction reaction in an acidic media I: Correlation between the ORR kinetic parameters and intrinsic physical properties of the alloys, J. Electroanal. Chem. 636 (2009) 1–9, https://doi.org/10.1016/j.jelechem.2009.06.023.
[14] S. Sharma, C. Zeng, A.A. Peterson, Face-centered tetragonal (FCT) Fe and Co alloys of Pt as catalysts for the oxygen reduction reaction (ORR): A DFT study, J. Chem. Phys. 150 (2019) 041704, https://doi.org/10.1063/1.5049674.
[15] Y. Li, J. Wang, X. Li, J. Liu, D. Geng, J. Yang, R. Li, X. Sun, Nitrogen-doped carbon nanotubes as cathode for lithium–air batteries, Electrochem. Commun. 13 (2011) 668–672, https://doi.org/10.1016/j.elecom.2011.04.004.
[16] P. Kichambare, S. Rodrigues, Mesoporous Nitrogen-Doped Carbon-LiSICON Glass Ceramics as High Performance Cathodes in Solid-State Lithium-Oxygen Batteries, Energy Tech. 1 (2013) 209–211, https://doi.org/10.1002/ente.201200028.
[17] C.H. Choi, S.H. Park, S.I. Woo, Binary and Ternary Doping of Nitrogen, Boron, and Phosphorus into Carbon for Enhancing Electrochemical Oxygen Reduction Activity, ACS Nano 6 (2012) 7084–7091, https://doi.org/10.1021/nn3021234.
[18] Z.-H. Sheng, H.-L. Gao, W.-J. Bao, F.-B. Wang, X.-H. Xia, Synthesis of boron doped graphene for oxygen reduction reaction in fuel cells, J. Mater. Chem. 22 (2012) 390–395, https://doi.org/10.1039/C1JM14694G.
[19] Y. Zhao, L. Yang, S. Chen, X. Wang, Y. Ma, Q. Wu, Y. Jiang, W. Qian, Z. Hu, Can Boron and Nitrogen Co-doping Improve Oxygen Reduction Reaction Activity of Carbon Nanotubes? J. Am. Chem. Soc. 135 (2013) 1201–1204, https://doi.org/10.1021/ja310566z.
[20] D.-S. Yang, D. Bhattacharjya, S. Inamdar, J. Park, J.-S. Yu, Phosphorus-Doped Ordered Mesoporous Carbons with Different Lengths as Efficient Metal-Free Electrocatalysts for Oxygen Reduction Reaction in Alkaline Media, J. Am. Chem. Soc. 134 (2012) 16127–16130, https://doi.org/10.1021/ja306376s.
[21] D. Yu, Y. Xue, L. Dai, Vertically Aligned Carbon Nanotube Arrays Co-doped with Phosphorus and Nitrogen as Efficient Metal-Free Electrocatalysts for Oxygen Reduction, J. Phys. Chem. Lett. 3 (2012) 2863–2870, https://doi.org/10.1021/jz3011833.
[22] Y. Sato, K. Itoh, R. Hagiwara, T. Fukunaga, Y. Ito, On the so-called “semi-ionic” C-F bond character in fluorine–GIC, Carbon 42 (2004) 3243–3249, https://doi.org/10.1016/j.carbon.2004.08.012.
[23] F. Yuan, W. Song, D. Zhang, Y.-S. Wu, Z. Li, H. Wang, W. Wang, Q. Wang, B. Wang, Semi-ionic C-F bond inducing fast ion storage and electron transfer in carbon anode for potassium-ion batteries, Sci. China Mater. 66 (2023) 2630–2640, https://doi.org/10.1007/s40843-022-2419-4.
[24] T. Jin, J. Chen, C. Wang, Y. Qian, L. Lu, Facile synthesis of fluorine-doped graphene aerogel with rich semi-ionic C-F bonds for high-performance supercapacitor application, J. Mater. Sci. 55 (2020) 12103–12113, https://doi.org/10.1007/s10853-020-04821-1.
[25] T. Ishizaki, Y. Wada, S. Chiba, S. Kumagai, H. Lee, A. Serizawa, O.L. Li, G. Panomsuwan, Effects of halogen doping on nanocarbon catalysts synthesized by a solution plasma process for the oxygen reduction reaction, PCCP 18 (2016) 21843–21851, https://doi.org/10.1039/C6CP03579E.
[26] D. Guo, R. Shibuya, C. Akiba, S. Saji, T. Kondo, J. Nakamura, Active sites of nitrogen-doped carbon materials for oxygen reduction reaction clarified using model catalysts, Science 351 (2016) 361–365, https://doi.org/10.1126/science.aad0832.
[27] J. Quílez-Bermejo, E. Morallón, D. Cazorla-Amorós, Oxygen-reduction catalysis of N-doped carbons prepared *via* heat treatment of polyaniline at over 1100 °C, Chem. Commun. 54 (2018) 4441–4444, https://doi.org/10.1039/C8CC02105H.
[28] A. Kulkarni, S. Siahrostami, A. Patel, J.K. Nørskov, Understanding catalytic activity trends in the oxygen reduction reaction, Chem. Rev. 118 (2018) 2302–2312, https://doi.org/10.1021/acs.chemrev.7b00488.
[29] Y. Taniguchi, Y. Shu, R. Takada, K. Miyake, Y. Uchida, N. Nishiyama, A zeolite templating method for fabricating edge site-enriched N-doped carbon materials, Nanoscale Adv. 5 (2023) 4233–4239, https://doi.org/10.1039/D3NA00186E.
[30] Y. Taniguchi, S. Kokuryo, R. Takada, X. Yang, K. Miyake, Y. Uchida, N. Nishiyama, Synthesis of pyridinic N-rich N-doped carbon by a zeolite template method using pyridine as a deposition source, Carbon Rep. (2023) 030101, https://doi.org/10.7209/carbon.030101.
[31] M. Cheng, R. Ma, G. Chai, Y. Chen, L. Bai, D. Wang, J. Qian, G.-H. Chen, Nitrogen-doped carbonized polyaniline (N-CPANI) for peroxydisulfate (PDS) activation towards efficient degradation of doxycycline (DOX) via the non-radical pathway dominated by electron transfer, Chem. Eng. J. 453 (2023) 139810, https://doi.org/10.1016/j.cej.2022.139810.
[32] W. Ren, G. Nie, P. Zhou, H. Zhang, X. Duan, S. Wang, The Intrinsic Nature of Persulfate Activation and N-Doping in Carbocatalysis, Environ. Sci. Tech. 54 (2020) 6438–6447, https://doi.org/10.1021/acs.est.0c01161.
[33] H. Nishihara, T. Kyotani, Zeolite-templated carbons – three-dimensional microporous graphene frameworks, Chem. Commun. 54 (2018) 5648–5673, https://doi.org/10.1039/C8CC01932K.
[34] H. Kiuchi, R. Shibuya, T. Kondo, J. Nakamura, H. Niwa, J. Miyawaki, M. Kawai, M. Oshima, Y. Harada, Lewis Basicity of Nitrogen-Doped Graphite Observed by CO2 Chemisorption, Nanoscale Res. Lett. 11 (2016) 127, https://doi.org/10.1186/s11671-016-1344-6.
[35] Y. Shu, R. Takada, Y. Taniguchi, X. Yang, K. Miyake, Y. Uchida, N. Nishiyama, Facile Synthesis of N-Doped Metal-Free Catalysts for Oxygen Reduction Reaction via a Self-Sacrificed Template Method Using Zinc Amino-Acid Complex, ACS Omega (2023) acsomega.3c07706. https://doi.org/10.1021/acsomega.3c07706.
[36] M. Li, Q. Ye, S. Hou, J. Yang, B. Chi, Y. Deng, X. Tian, Fluorine and phosphorus atoms cooperated on an N-doped 3D porous carbon network for enhanced ORR performance toward the zinc–air batteries, J. Mater. Chem. A 11 (2023) 8730–8738, https://doi.org/10.1039/D2TA09792C.
[37] J. Quílez-Bermejo, M. Melle-Franco, E. San-Fabián, E. Morallón, D. Cazorla-Amorós, Towards understanding the active sites for the ORR in N-doped carbon materials through fine-tuning of nitrogen functionalities: an experimental and computational approach, J. Mater. Chem. A 7 (2019) 24239–24250, https://doi.org/10.1039/C9TA07932G.